Intertwined string orders of topologically trivial and nontrivial phases in an interacting Kitaev chain with spatially varying potentials

Weijie Huang [1] and Yao Yao [1,2,*]

[1] *Department of Physics, South China University of Technology, Guangzhou 510640, China*

[2] *State Key Laboratory of Luminescent Materials and Devices, South China University of Technology, Guangzhou 510640, China*

(Received 16 December 2021; revised 22 May 2022; accepted 15 June 2022; published 28 June 2022)

By using the variational matrix product state method, we numerically study the interacting Kitaev chain with spatially varying periodic and quasiperiodic potentials, and the latter follows the Fibonacci sequence. The edge correlation functions of Majorana fermions and low-lying ground states are computed to explore the robustness of topological superconducting phase. It is found that the original topologically nontrivial phase is separated into two branches by an emergent topologically trivial phase, as a result of the competition among spatially varying potential, electronic, Coulomb interaction, and chemical potential. The analysis of energy gap, occupation number, and intertwined string order parameters together suggests that the lift of degeneracy in the topologically trivial phase is enabled by a potential-induced fracton mechanism, namely, the pairing of four Majorana fermions. The evolution from the emergent fractal structure of population to the original structure of charge density wave is investigated as well.

DOI: 10.1103/PhysRevB.105.245144

I. INTRODUCTION

In the last decade, Majorana zero mode (MZM), a special kind of fermion, has attracted much attention in condensed matter physics, quantum computations, and other related fields [1–4], for both its quantum properties originating from non-Abelian statistics [5] and the potential to be robust qubits [6,7]. Consequently, the realization and control of MZMs turn out to be an appealing subject. A number of realistic systems have been proposed [8–18] for hosting MZMs and extensive experiments [19–28] have been conducted on them. On the theoretical side, the Kitaev chain was introduced based upon spinless p-wave superconductivity in one dimension [8], which is one of the simplest but nontrivial models to unveil MZM. The most exotic features of this Kitaev chain are the exponential localization of Majorana edge modes at the chain's ends.

Up to date, researchers have devoted great effort to the stable topological phase exhibiting the MZMs. The studies extended to issues of nearest-neighboring repulsive interactions [29–33], long-range interactions [34–36], quartic interactions [37], dimerization [38], disorder [39–44], quasiperiodicity [42,45], and so on. Considering interactions, the phase diagram of the Kitaev chain has become one of the most active topics. Various theoretical methods [30–32,37,46] have been achieving consensus on the phase boundaries among trivial superconductor (SC), topological superconductor (TSC), commensurate charge density wave (CDW), incommensurate charge density wave (ICDW), and Schrödinger-cat state (CAT). Whereas, there are still more phases to be found, as some of the hidden symmetries in the model have not been uncovered. For example, a recent work [47] discovered a novel phase between the ICDW and CDW phases, named "excited state charge density wave (es-CDW)," in which the ground state resembles the excited states of CDW phase. Furthermore, it was also found that moderate interactions generally broaden the surviving window of chemical potential for the TSC phase [30–33,37,46].

On the other hand, MZMs were also found to survive broader parameter regions in inhomogeneous chains with disorder or quasiperiodicity than that in the ordered cases [42,48,49]. The quasiperiodic potential will result in the fractal structures in the wave function whose intrinsic topology will influence the MZMs [50]. The simplest model for quasiperiodicity is the Harper model [51] with a cosinelike shaped potential, which has been considered in Kitaev chains [45,49,52] and a fractal structure similar to Hofstadter's butterfly have been observed [42]. The potential following Fibonacci sequence is another possible realization for quasiperiodicity. It was proven that the Fibonacci potential can be obtained using a superposition of Harper potentials [53–56]. A new self-similar fractal structure was then found in the topological phase diagram of the Kitaev chain with Fibonacci potential (Fibonacci-Kitaev chain) [57].

Consequently, both interactions and inhomogeneous potentials serve as the two most essential ingredients to the relevant experiments. So far, it has been proven that either moderate disorders or repulsive interactions are able to stabilize the topological order, but when the disorders are sufficiently strong, interactions always suppress the topological phase no matter repulsive or attractive [58]. While comparable, however, the interplay of interactions and disordered and quasiperiodic potentials is much less understood [39,41,52,58]. As we always believe, nontrivial effects on the topological phase could emerge in this parameter region, so more detailed studies are highly demanded.

*yaoyao2016@scut.edu.cn

In this paper, we study the Kitaev chain with both Fibonacci potential and interactions. The Fibonacci potential is composed of two tiles of different potential values. Specifically, we assign the one of the tiling potential to be zero and leave the other nonzero. Additionally, we also consider sites with zero potential following the periodic or other quasiperiodic sequences. By using the variational matrix product state (VMPS) method, also known as the matrix product states version of density-matrix renormalization group (DMRG), we calculate several observables to study the phase transition. The edge correlation function of the two Majorana operators at the edges is used as a long-range-order parameter to characterize the nontrivial TSC phase with MZMs. We find a topologically trivial phase appears to divide the TSC phase into two branches. By calculating the low-lying ground state of two different parity sectors [59], we find this topologically trivial phase has a nondegenerate ground state with intertwined orders and propose two kinds of string order parameters to describe them. We also calculate the occupation with different parameters. Results are in good agreement in the two cases: the potential of periodic sequence and quasiperiodic Fibonacci sequence. These chains have adjacent sites with zero chemical potential, so it may be closely relevant to the fracton physics [60–64].

II. MODEL

A. Kitaev model and JW transformtion

Let us begin with the benchmarking Kitaev model for spinless fermions with open boundary condition [8]. The Hamiltonian is written as

$$H=\sum_{j=1}^{L-1}[-t(c_j^\dagger c_{j+1}+\text{H.c.})+U(2n_j-1)(2n_{j+1}-1) -\Delta(c_j^\dagger c_{j+1}^\dagger+\text{H.c.})]-\sum_{j=1}^{L}\mu_j\left(n_j-\frac{1}{2}\right), \quad (1)$$

where the operator $c_j^\dagger$ (c_j) creates (annihilates) a spinless fermion on jth site, $n_j=c_j^\dagger c_j$ is the corresponding fermion occupation operator, t is the hopping amplitude, Δ is the p-wave superconducting pairing potential, μ_j is the chemical potential on jth site, and U is the nearest-neighbor interaction. Without loss of generality, we can assume that t and μ to be real and positive since $t\to -t$ and $\mu\to -\mu$ and be realized by the gauge transformation $c_j\to i(-1)^j c_j$ and particle-hole conjugation $c_j\to(-1)^j c_j^\dagger$, respectively, and these transformations do not change other parameters.

It is well known that this Hamiltonian can be represented in the Majorana fermion form. That is, a complex fermion operator can be split into two Majorana fermion operators:

$$c_j=\tfrac{1}{2}\left(\lambda_j^1+i\lambda_j^2\right), \quad (2)$$

$$c_j^\dagger=\tfrac{1}{2}\left(\lambda_j^1-i\lambda_j^2\right). \quad (3)$$

The Majorana fermion operators satisfy the Majorana condition $(\lambda_j^a)^\dagger=\lambda_j^a$ and also obey the anticommutation relation $\{\lambda_j^a,\lambda_l^b\}=2\delta_{ab}\delta_{jl}$, where $a,b=1,2$. So the Hamiltonian (1) can be transformed to the following form:

$$H=\sum_{j=1}^{L-1}\Big[-\frac{i}{2}(t+\Delta)\lambda_{j+1}^1\lambda_j^2-\frac{i}{2}(t-\Delta)\lambda_j^1\lambda_{j+1}^2 -U\lambda_j^1\lambda_j^2\lambda_{j+1}^1\lambda_{j+1}^2\Big]-\frac{i}{2}\sum_{j=1}^{L}\mu_j\lambda_j^1\lambda_j^2. \quad (4)$$

Furthermore, one can use the Jordan-Wigner (JW) transformation to construct spin operators:

$$S_j^x=\tfrac{1}{2}\lambda_j^1 e^{i\pi\sum_{l<j}n_l}, \quad (5)$$

$$S_j^y=-\tfrac{1}{2}\lambda_j^2 e^{i\pi\sum_{l<j}n_l}, \quad (6)$$

$$S_j^z=\frac{i}{2}\lambda_j^1\lambda_j^2. \quad (7)$$

When $\Delta=t$, the Hamiltonian (4) can be further mapped to a spin-chain Hamiltonian which is written in terms of spin operators S_j^x and S_j^z, i.e.,

$$H=\sum_{j=1}^{L-1}-4tS_j^xS_{j+1}^x+4US_j^zS_{j+1}^z+\sum_{j=1}^{L}\mu_jS_j^z. \quad (8)$$

This form of Hamiltonian is friendly to the numerical approaches.

B. Symmetries

In presence of the pairing term, the total fermion number $\hat{N}=\sum_j n_j$ is not conserved. However, the Hamiltonian commutes with the fermion number parity Z_2^f defined as

$$Z_2^f=e^{i\pi\sum_j n_j}=(-1)^{\hat{N}}. \quad (9)$$

In addition, the particle-hole symmetry can be characterized by the particle-hole conjugation operator defined as

$$Z_2^p=\prod_j[c_j+(-1)^j c_j^\dagger], \quad (10)$$

which is also conserved if and only if $\mu=0$. We can use these two symmetries Z_2^f and Z_2^p of the ground states to distinguish different phases.

Usually there are three topologically trivial phases including trivial superconductor, CDW, and ICDW. The TSC phase has opposite fermion number parity Z_2^f in the twofold-degenerate ground states while the CDW and ICDW phase have the same Z_2^f. The CDW can be distinguished from ICDW by local occupation number distribution and its Fourier spectrum. The ground state changes from trivial superconductor to TSC, ICDW, and CDW by increasing U [59].

C. Quasiperiodic potential

The models under study in the next section are the interacting Kitaev chains with different types of spatial varying chemical potentials. We assign each μ_i by either μ_A or

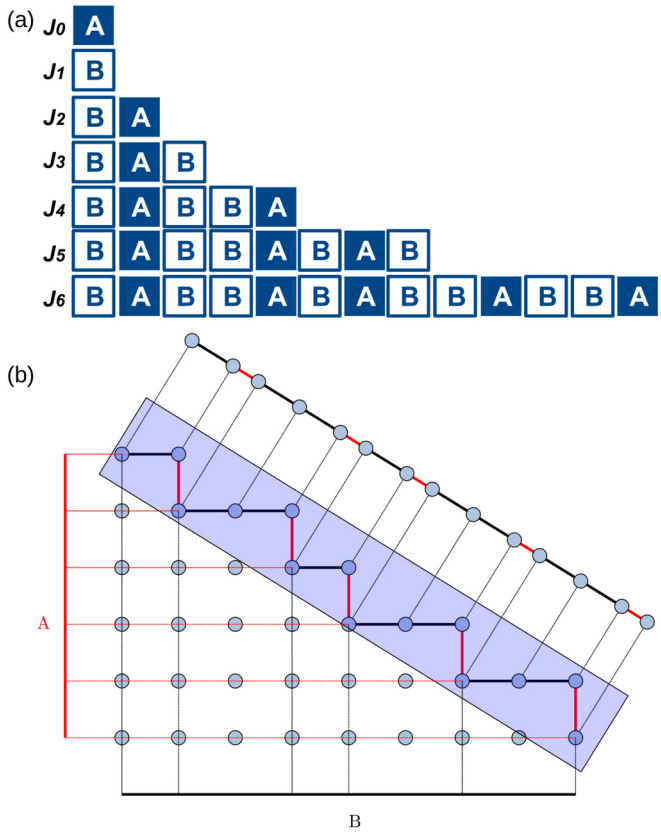

FIG. 1. (a) The first seven Fibonacci sequences depicted as horizontal chains labeled by J_n. A and B represent that the relevant chemical potentials are μ_A and μ_B, respectively. (b) The Fibonacci chain can also be obtained by cutting the square lattice with a strip and projecting it on a straight line.

μ_B. The periodicity and quasiperiodicity in μ_i are given by making the order of A and B follow the periodic or quasiperiodic sequences. We mainly focus on the lattices with chemical potential following the quasiperiodic Fibonacci sequence [57,65]. One can use the following recursion formula to get the sequence composed of two symbols A and B. That is, we use the recursion formula $J_{n+1} = \{J_n, J_{n-1}\}$, $n \geqslant 1, J_0 = \{\mathrm{A}\}, J_1 = \{\mathrm{B}\}$, so we have $J_2 = \{J_1, J_0\} = \{\mathrm{B}, \mathrm{A}\}$, $J_3 = \{J_2, J_1\} = \{\mathrm{B}, \mathrm{A}, \mathrm{B}\}, \ldots$. The total number of symbols in J_n is given by the Fibonacci numbers $F_{n+1} = F_n + F_{n-1}$. Figure 1(a) displays the first seven Fibonacci sequences and Fig. 1(b) shows the Fibonacci chain with J_6 which can be obtained by the cutting approach [57,66]. All the dots within the strip on the two-dimensional (2D) square lattice are connected and projected orthogonally to a line parallel to the strip. The projection of the red vertical lines and black horizontal lines within the strip yield two values of distances in the resultant line, representing the A symbols and B symbols in the Fibonacci sequences, respectively.

For the actual value of μ_A and μ_B in the following calculation, we will set one of them to be zero ($\mu_A = 0$ or $\mu_B = 0$) and vary the other one. The chemical potential μ_i at adjacent sites might both be zero in some situations. This will presumably lead to unique results.

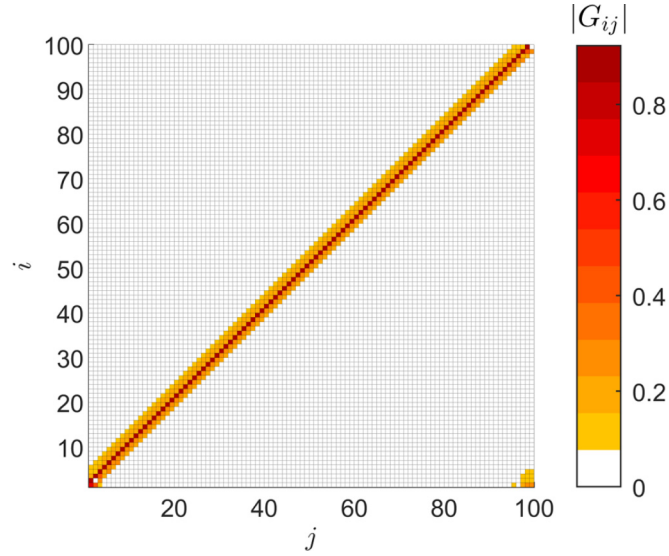

FIG. 2. Correlation function G_{ij} for the TSC ground state with $\Delta = t, \mu = 0, U = 0.5t, L = 100$. The existence of the edge modes is fingerprinted by the finite G_{1L} value appearing at the bottom right corner.

III. RESULTS

In this work, we use variational matrix product state (VMPS) [67–69] to study the interplay of the nearest interaction and quasiperiodic chemical potential. In the previous researches, various fingerprints have been employed to quantify the phase diagram, including entanglement entropy and entanglement spectrum [37,47,58,70–73], Lyapunov exponent [42,57,74], string correlation function [29,49,58,59,70,75], many-body Majorana operator [76,77], Hartree-Fock analysis [37], lowing-energy spectrum/gap [40,47,70,72,78–82], and tunneling spectra [32]. Here, we compute several observables, including the energy of low-lying states, local particle density, and most importantly the edge correlation function [59]. The correlation function between two sites i and j is defined as

$$G_{ij} = \langle i\lambda_i^1 \lambda_j^2 \rangle. \tag{11}$$

In particular, when $i = 1$ and $j = L$ it is the edge component of G_{ij}, i.e.,

$$G_{1L} = \langle i\lambda_1^1 \lambda_L^2 \rangle, \tag{12}$$

which is straightforwardly related to the edge modes. A typical result of G_{ij} is shown in Fig. 2. It is worth noting that the correlation function G_{ij} is a block matrix of electron or hole density, which can be generalized to interacting systems and reflects the site distribution of single-particle elementary excitations in a many-body ground state. As long as the bulk is homogeneous, in the thermodynamic limit a finite value of G_{1L} fingerprints the existence of edge modes since the correlation can not be transferred site by site to such long distance. One may then wonder how about the inhomogeneous lattice? In this work, we thus calculate G_{1L} with spatially varying chemical potential, which will lead the bulk to be inhomogeneous. The nonvanishing edge correlation function $G_{1L} = \langle i\lambda_1^1 \lambda_L^2 \rangle$ characterizes the topological order, that is, the value

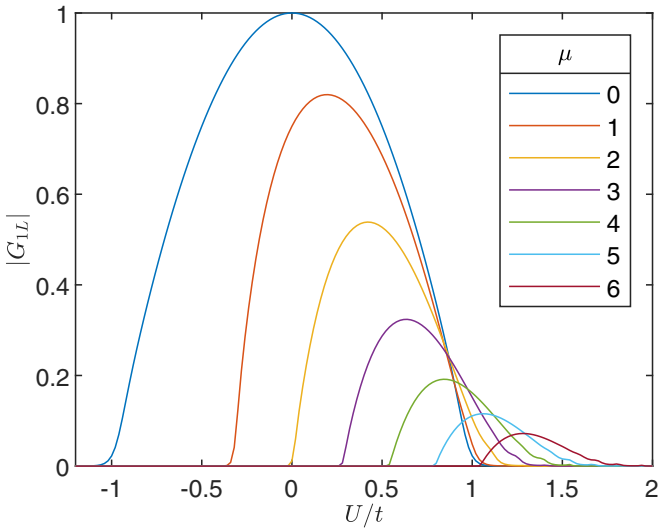

FIG. 3. Edge correlation function G_{1L} of the ground state of the interacting Kitaev chain as a function of μ and U. The chemical potential is uniform and $\Delta = t$, $L = 88$.

G_{1L} is finite in TSC phase and vanishes in other topologically trivial phases, and also this order parameter is valid both in noninteracting and interacting systems. Fixing $\Delta = t$, we can plot the ground-state edge correlation G_{1L} of the interacting Kitaev chains as a function of U.

A. Periodic chemical potential

We first calculate the edge correlation function of the interacting Kitaev chain with 88 sites. Two cases without and with periodic chemical potentials are considered, with the results shown in Figs. 3 and 4, respectively, for comparison. We notice that, since the model hosts MZMs on the edges, the

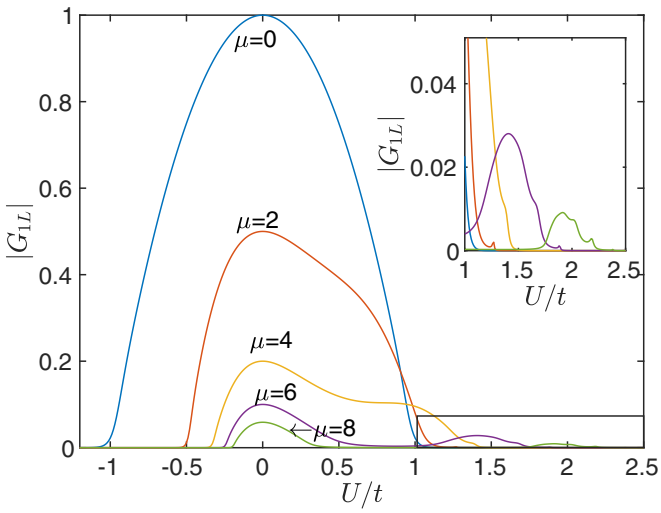

FIG. 4. Edge correlation function G_{1L} of the ground state with periodic chemical potential as functions of μ and U. $L = 88$, $\Delta = t$, $[\mu, 0, 0]$ as the repeated form for the chemical potential on sites 1 to 87, and let the last site $\mu_L = \mu$. Region in the black box is zoomed in and illustrated in the inset.

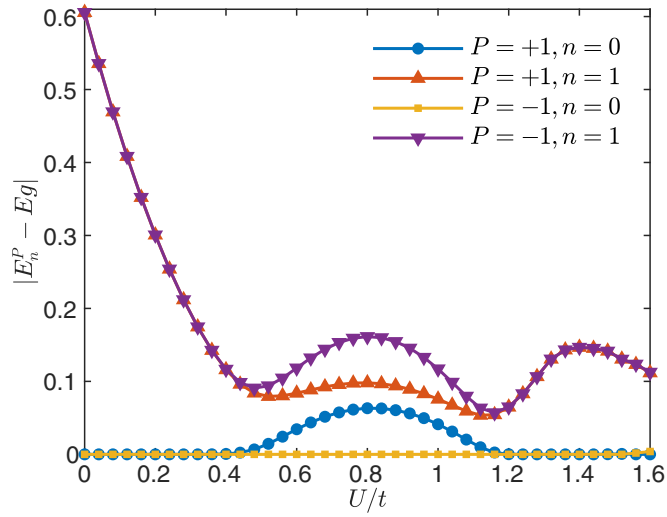

FIG. 5. Energy with respect to the ground state $E_n^p - E_g$. The ground state ($n = 0$) and the first excited state ($n = 1$) of two parity sectors of Z_2^f are calculated in the periodic chain with $\mu = 6$, $\Delta = t$, $L = 88$. We set $[\mu, 0, 0]$ as the repeated form for the chemical potential on sites 1 to 87, and let the last site $\mu_L = \mu$.

chemical potential on the end site of the chain is extremely important [47]. The periodic chemical potential is repeated from site 1 to 87 with a period of $[\mu, 0, 0]$, and we set $\mu_{88} = \mu$ to make the last site the same as the first site. This particular periodic potential pattern is chosen to make it easier to compare with the quasiperiodic potential studied in the next section.

The results shown in the two figures are remarkably different. In Fig. 3, increasing the chemical potential μ makes the maximum value of G_{1L} decrease and shifts the regions with nonvanishing G_{1L} to the right where the interaction is stronger. In Fig. 4, however, G_{1L} manifests its maximum value with no interaction and survives even large chemical potential. More importantly, for a given μ there is a valley between two peaks, indicating the TSC phase is separated into two branches. This phenomenon means the phase diagram changes to a pattern which is rather different from that in previous researches [29,31,32,47,59]. It is noteworthy that this effect is more evident with larger chemical potential.

As the VMPS or DMRG method often encounter the boundary problem, that will affect the accuracy of using the edge correlation function to determine the phase transition point. We then analyze the symmetries in the ground-state phase transition for comparison. The fermion number parity Z_2^f conserves in this model which means the Hilbert space will be divided into two parity sectors denoted by $P = +1, -1$. The TSC phase has opposite fermion number parity Z_2^f in the twofold-degenerate ground states while the charge density wave (CDW) and incommensurate charge density wave (ICDW) phase have the same Z_2^f. The lowest two eigenstates, which are the ground state ($n = 0$) and the first excited state ($n = 1$) in each parity sector, are represented in Fig. 5. The analysis of symmetries of the ground state consists with the results of the edge correlation function that the TSC phase does split into two. No

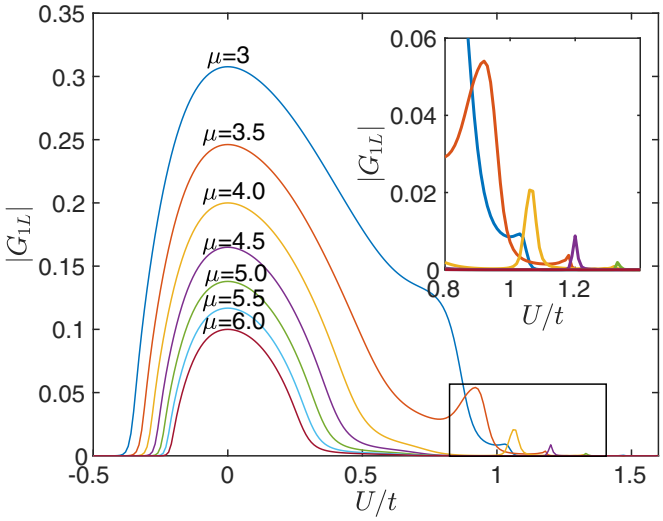

FIG. 6. Edge correlation function G_{1L} of the ground state of the interacting Fibonacci-Kitaev chain as functions of μ and U with $L = 88$, $\Delta = t$, $\mu_A = \mu$, $\mu_B = 0$, and $\mu_1 = \mu_L = \mu$. The Fibonacci sequence J_{10} containing 89 sites is used to generate quasiperiodic potential with $\mu_1 = 0$, $\mu_{89} = \mu$. The first site with zero potential is discarded to make potential nonzero at both ends of the chain, so the chain has $\mu_1 = \mu_L = \mu$ with $L = 88$. Region in the black box is zoomed in and illustrated in the inset.

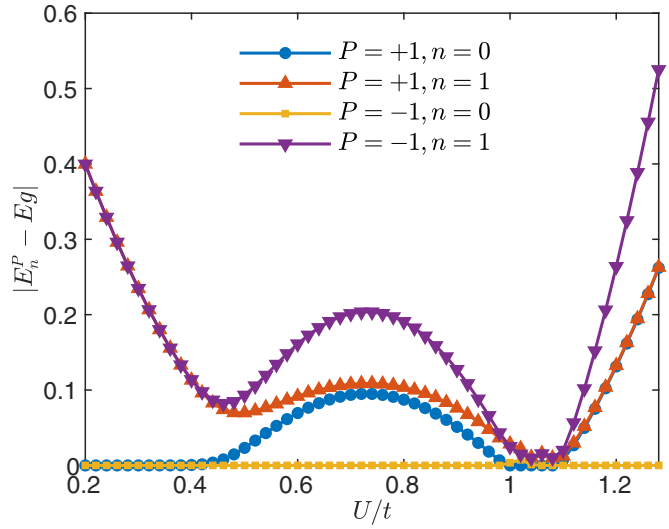

FIG. 7. Energy with respect to the ground state $E_n^p - E_g$. The ground state ($n = 0$) and the first excited state ($n = 1$) of two parity sectors of Z_2^f are calculated in the interacting Fibonacci-Kitaev chain with $\mu = 4$, $\Delta = t$, $L = 88$.

degeneracy is found between the two TSC phases which is completely different from all the phases in the uniform interacting Kitaev chain [59], which will be extensively discussed below.

B. Quasiperiodic chemical potential

We are now interested in the situations if we use quasiperiodic sequences to substitute the periodic sequence. As it equivalently introduces moderate disorders to the system, one may image the split of the TSC phase probably would not show up. To this end, we use the Fibonacci sequence J_{10} containing 89 sites to generate quasiperiodic chemical potential and discard the first site in J_{10}, so the chain contains 88 sites and has nonzero chemical potential on both ends. The results are shown in Fig. 6. It is found that all the results are similar with those in the periodic case displayed in Fig. 4. The edge function G_{1L} with $\mu > 3$ also behaves a second growth as the repulsive interaction increases, where G_{1L} can even decrease to around zero between two peaks for several μ values. Fixing μ, there is a trivial region between two topological regions that is completely identical to the periodic case. Nonetheless, one can observe it more clearly in Fig. 6 that the TSC phase gradually breaks into two branches with the chemical potential increasing. The quasiperiodicity does not essentially kill or suppress the emergency of two topological regions. When the interaction is small, the TSC state even becomes stabler in the periodic and quasiperiodic chains than that in the uniform chain. The moderate disorder brought by the quasiperiodic potential broadens the chemical potential window in the noninteracting chain ($U = 0$), same with the previous results [30–32,37,46].

Chains with more sites are calculated as well. That is, we use J_{11} and J_{12} to generate Fibonacci chains with 144 and 232 sites. The G_{1L} near the phase boundaries are influenced by the length of the chain. But, the location and the size of the second TSC phase keeps the same for chains with different length, suggesting the phase diagrams are all the same for these chains. The G_{1L} decreases to zero more quickly in longer chains which makes the phase boundary more precise. Totally speaking, the exact phase boundary is difficult to exactly identify by just looking at the vanishing G_{1L}. For this reason, it should be better to use the inflection point of G_{1L} as the phase boundary, following the normal treatment of T_c in superconductors. We do not show results for more sites since the numerical calculation is hard to converge even if we kept bond dimension $\kappa = 400$ and run 100 sweeps.

The lowest two eigenstates of the Fibonacci-Kitaev chain in both parity sectors are displayed in Fig. 7. Unlike the edge correlation function, the eigenstates for the quasiperiodic case is fairly different with the periodic case. For $U \lesssim 0.5$ and $1.0 \lesssim U \lesssim 1.1$, the ground state is doubly degenerate with opposite parity implying the chain is in a gapped topological superconducting phase. For $0.5 \lesssim U \lesssim 1.0$, the degeneracy is lifted and the intertwined string orders emerge which might prefer to a new topologically trivial phase without superconductivity. The appearance of this exotic phase leads to the split of the TSC phase. The energy gap of this topologically trivial phase is incredibly small, which is of the order 10^{-4} per site in the unit of hopping amplitude t. For $U \gtrsim 1.1$, the $P = 1$ sector has degenerate ground states while the other parity sector has got a gap between the ground state and the first excited state. But the unique ground state with the $P = -1$ has CDW ordering and this gap will eventually close while U increases. In other words, the ground state will eventually change into the CDW/ICDW phase having doubly degenerate states with different party if we keep increasing the interaction U.

We notice that there has been a research focusing on the region near the phase boundary and discussing the

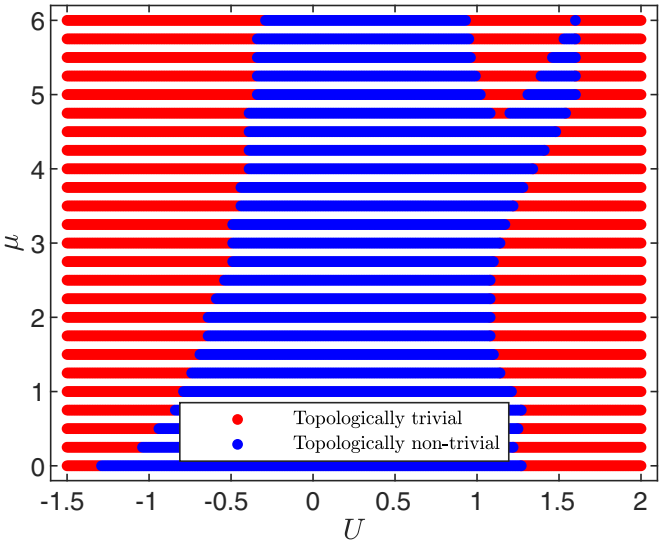

FIG. 8. Phase diagram for the interacting Fibonacci-Kitaev chain. Data points obtained in the same quasiperiodic chain as Fig. 6 with $L = 88$, $\Delta = t$, $\mu_A = \mu$, $\mu_B = 0$, and $\mu_1 = \mu_L = \mu$. The edge correlation function G_{1L} of the blue dots is nonvanishing which is in the topological superconductor phase and G_{1L} of the red dots are less than 10^{-6} that is in topologically trivial phase.

degeneracy and the parity of the ground state for different system sizes [47]. Apart from the previously reported phases, a newly observed "excited state charge density wave" (es-CDW) phase is present in that work. They found the esCDW exists between the ICDW phase and the CDW phase and had been considered to be part of the CDW phase. They use "es" because the ground state in this phase does not possess the conventional CDW ordering but its properties resemble the properties of the excited states in CDW phase. A more interesting point is that the esCDW phase appears only for even system sizes and is sensitive to the chemical potential at the edges. Furthermore, the transition point from this new phase to the CDW phase can actually be governed by the chemical potentials at the two edges. More analysis of two lowest states in each parity sector can be found in this research. An exotic nondegenerate phase without the limitation of system size is found when we use the nonuniform chemical potentials. Our results turn out to be an exotic finding in addition to it.

C. String ordering

The stability of the topological order is related to all terms in the model, and the exact phase boundary is pretty difficult to determine. The phase diagrams of the uniform chain obtained by various methods have essentially the same pattern [30–32,37,46]. Using the edge correlation function as a criterion, different phases can be then quantitatively assigned. The resulting phase diagram of chains with Fibonacci quasiperiodic potential is subsequently sketched in Fig. 8. It has several fascinating differences from that for the uniform chain. As displayed in Fig. 3, the TSC phase of the uniform interacting Kitaev chain with larger μ tends to demand stronger interaction, where the $\mu = 0$ curve has got slight overlap with the $\mu = 6$ curve. But in Fig. 8 the TSC phase with different μ is restricted within a small range in the horizontal axis and piled up in the vertical axis. Especially, it is obvious in former results that there is an upper limit of chemical potential for the TSC phase to survive when the interaction strength is zero ($U = 0$). However, this limit disappears in Fig. 8 and the system can still stay in the TSC phase with Fibonacci quasiperiodic chemical potential up to an extremely large value. And also we can find for $\mu > 4.75$, the topological phase is divided into two branches with a topologically trial phase in-between. That is to say the second peak in Fig. 6 will result in the peninsulalike area in the phase diagram, which is the most distinctive difference from the uniform chain [30–32,37,46].

As stated, the transition of these topological phases is dominated by the parity symmetries Z_2^f and Z_2^p, which are defined by string operators in product form. If we directly calculate the expectation values of string operators, however, the long-range ordering is not featured. This is because Z_2^p is actually the alternating product of S_x and S_y operators, and the action of S_y on X site vanishes. On the other hand, via JW transformation, λ_1 and λ_2 operators are transformed to S_x and S_y, respectively, so in the topological phases the nearest sites are not exactly X-X pairing while the next nearest are. To this end, we define two string order parameters as

$$O_{ji}^x = \left\langle S_j^x I_{j+1} S_{j+2}^x I_{j+3} S_{j+4}^x \ldots I_{i-1} S_i^x \right\rangle, \tag{13}$$

$$O_{ji}^z = \left\langle S_j^z I_{j+1} S_{j+2}^z I_{j+3} S_{j+4}^z \ldots I_{i-1} S_i^z \right\rangle, \tag{14}$$

where $j < i$ and both of them are currently even or odd. We then call them Z string and X string, respectively, to characterize Z_2^f and Z_2^p symmetries.

For a simple interacting Kiteav chain with $\mu = 0$, both the symmetries Z_2^f and Z_2^p are conserved. It has been stated that [75] in the topological phase (TSC) the degeneracy is protected by edge modes so the ground state will fall into different number parity sectors by spontaneous symmetry breaking, while in topologically trivial phase (CDW/ICDW) it goes to different electron-hole parity sectors. We further observe that (not shown), the X-string order dominates with $U < 1.0$ where the system is in topological phase. As U increases, the X string order parameters will decrease while the Z-string order parameters will increase. The X string and Z string become nearly the same at $U = 1.0$, and the Z string overtakes X string when $U > 1.0$. The system experiences a phase transition at $U = 1.0$ from the topological phase to the topologically trivial phase (CDW/ICDW phase). Thus, the X-string order parameter can be used to measure the topological order and the Z-string order parameter can be used to measure the topologically trivial order.

The expectation values of the X string and Z string in the interacting Fibonacci-Kitaev chain are represented in Fig. 9. For $U < 0.5$ or $U > 1.0$, one of the string order parameters dominates so that the ground state is doubly degenerate with opposite (TSC phase) or same (CDW/ICDW phase) fermion number parity Z_2^f. But for $0.5 < U < 1.0$, the X-string order is compatible with the Z-string order, implying two kinds of string orders are intertwined in this region. As a result, the degeneracy of the ground state is lifted in this region. Outside

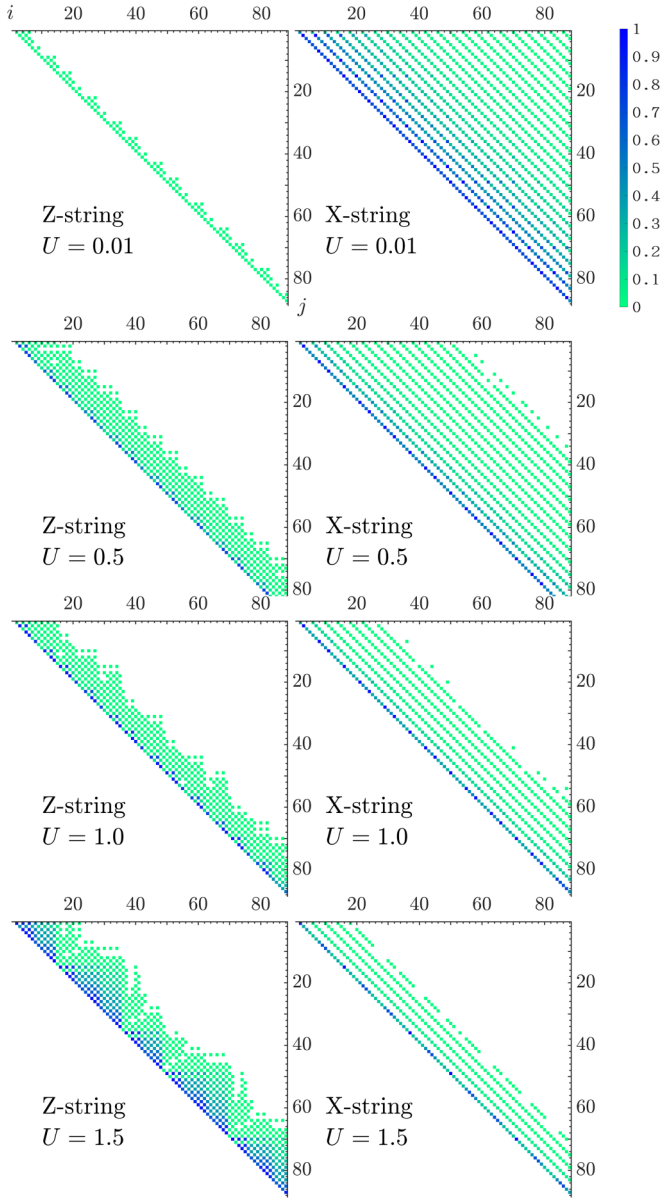

FIG. 9. The expectation values of the Z string and X string in the interacting Fibonacci-Kitaev chain with $\mu = 4.0$, $L = 88$.

this region, one of the three terms in the Hamiltonian will dominate and lead to a single string order.

D. Fractal structure

In the uniform interacting Kitaev chain, the occupation number decays drastically following μ increasing. The repulsive interaction prefers the ground states with occupation number having patterns like $(1010\ldots)$ and $(0101\ldots)$, which is expected to find in the phase of CDW. As the interaction becomes stronger the total occupation number will approach $N_{\text{tot}} = L/2$, the chemical potential will compete with the repulsive interaction. From Fig. 10 one can see the sites with $\mu_b = 0$ are half-occupied. We observe that the adjacent sites with $\mu = 0$ collect four Majorana fermions as a group, allowing the two fermions to move along the chain just like the mechanism of fractons [60–64]. Consequently, the total

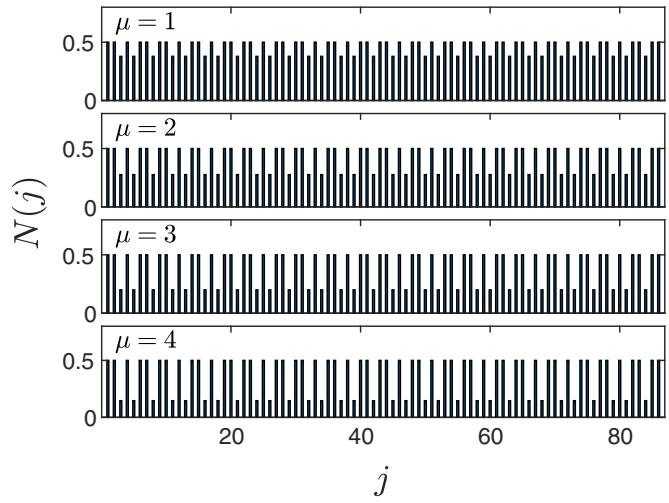

FIG. 10. Occupation number $N(j) = \langle n_j \rangle$ of Fibonacci-Kitaev chain without interaction ($U = 0$) of $\mu = 1, 2, 3, 4$. The system size $L = 88$, $\Delta = t$, $\mu_a = \mu$, $\mu_b = 0$, and $\mu_1 = \mu_L = \mu$.

occupation number is larger than in the normal interacting chain that the chemical potential window is broadened even further. It is intriguing that one can find the occupation number is nearly the same for $U = 0.4, 0.8, 1.2$ in Fig. 11, namely, the topologically trivial phase with $U = 1.2$ has the same occupation number distribution as the two branches of the nontrivial phase adjacent to it. More thorough investigations are needed for us to identify and understand properties of the exotic topologically trivial phase.

The Fourier spectrum is thus obtained by taking fast Fourier transformation of the local occupation number $N(j) = \langle n_j \rangle$. The quasiperiodicity brought by the spatial varying potential can be most readily seen in Fourier spectrum [83]. For the Fourier spectrum of the $U = 0$ chain in Fig. 12, the intensity is symmetric about $k = \pi$ and exhibits a fractal structure originated from the Fibonacci sequence. The fractal structure in the Fourier spectrum is

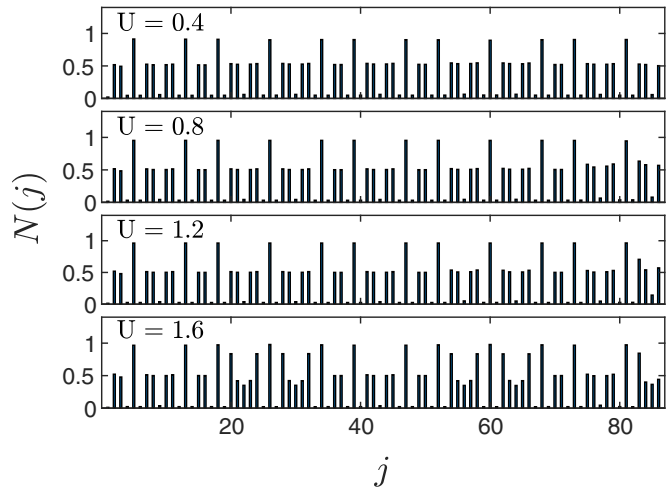

FIG. 11. Occupation number $N(j) = \langle n_j \rangle$ of interacting Fibonacci-Kitaev chain with $\mu = 6$ and interaction $U = 0.4$, 0.8, 1.2, 1.6. The system size $L = 88$, $\Delta = t$, $\mu_a = \mu$, $\mu_b = 0$, and $\mu_1 = \mu_L = \mu$.

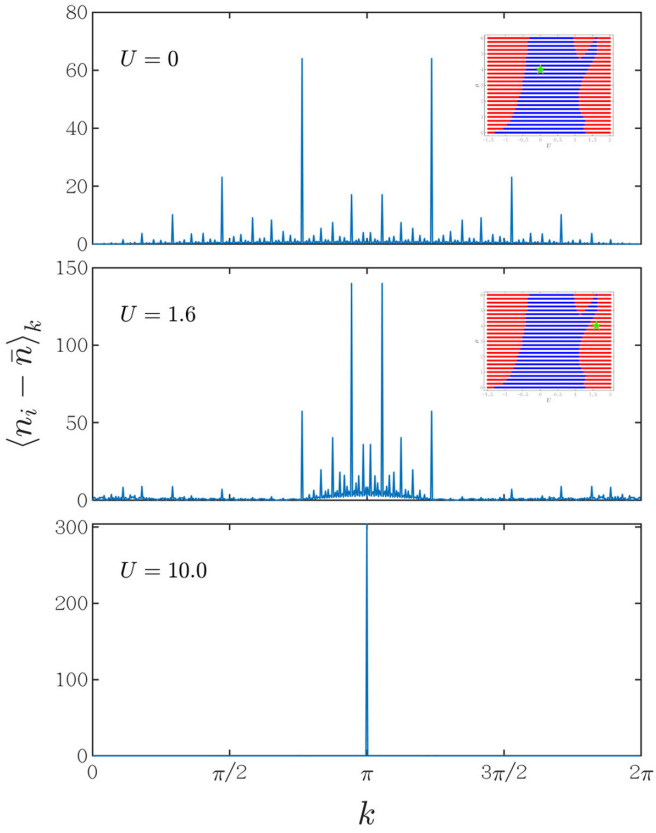

FIG. 12. Fourier spectrum of the occupation number $N(j) = \langle n_j \rangle$ of interacting Fibonacci-Kitaev chain with $\mu = 4$, $L = 610$, $\Delta = t$, and $U = 0.0, 1.6, 10.0$. The green pentagrams in the insets are their corresponding positions on the phase diagram.

destroyed by the interaction and evolved to the CDW structure. Increasing the interaction U, the prominent peaks around $k = \pi$ will get closer and have stronger intensity, and subsequently there exists only a single peak in Fourier spectrum at $k = \pi$ corresponding to an occupation number distribution of CDW phase.

The edge correlation function is more sensitive to the chemical potential at the edge rather than the system size. In order to examine it, we use different length of Fibonacci sequence (up to J_{13}) and conclude that the chains with $\mu = 0$ at both boundaries have edge correlation function $G_{1L} \approx 1$ when the interaction is small, which is distinct from the other three sets shown in Fig. 13. This is also valid to the chain with quasiperiodic chemical potential following other sequences such as the Thue-Morse sequence as shown in Fig. 13. For the Thue-Morse lattice, we use recursion formula $S_{n+1} = \{S_n, S_n^{-1}\}$, $n \geqslant 1$, $S_0 = \{\mathrm{A}, \mathrm{B}\}$, so we have $S_1 = \{S_0, S_0^{-1}\} = \{\mathrm{A}, \mathrm{B}, \mathrm{B}, \mathrm{A}\}$, $S_2 = \{S_1, S_1^{-1}\} = \{\mathrm{A}, \mathrm{B}, \mathrm{B}, \mathrm{A}, \mathrm{B}, \mathrm{A}, \mathrm{A}, \mathrm{B}\}, \ldots$. The total number of symbols is S_n is $G_n = 2G_{n-1} = 2 \times 2^n$. It is found that, although there are some differences for the four kinds of chemical potentials at the edge, respectively, following the Fibonacci sequence and the Thue-Morse sequence, the latter leads to equivalent results and the exotic topologically trivial phase does survive all of them.

Generally speaking, all the three potentials we are studying exhibit almost the same behaviors with negligible distinctions. It means the configuration of potential and disorder almost

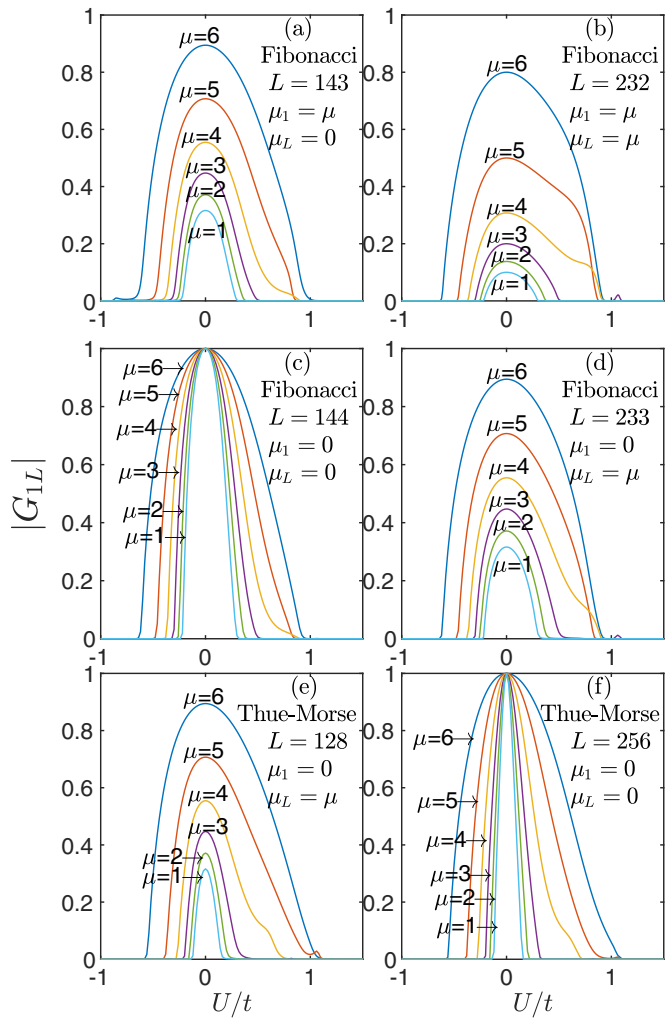

FIG. 13. Edge correlation function G_{1L} of ground state of the interacting Kitaev chain with different types of chemical potentials. Whereas $\Delta = t$, $\mu_A = \mu$, $\mu_B = 0$. (a) Fibonacci lattice, $L = 143$, $\mu_1 = \mu$, $\mu_L = 0$. (b) Fibonacci lattice, $L = 232$, $\mu_1 = \mu_L = \mu$. (c) Fibonacci lattice, $L = 144$, $\mu_1 = \mu_L = \mu$. (d) Fibonacci lattice, $L = 233$, $\mu_1 = 0$, $\mu_L = \mu$. (d) Thue-Morse lattice, $L = 233$, $\mu_1 = 0$, $\mu_L = \mu$. (d) Thue-Morse lattice, $L = 233$, $\mu_1 = 0$, $\mu_L = \mu$.

does not matter. The competition between the interaction and the chemical potential by itself can not explain the emergence of the intertwined string orders which is different from all other known situations. It deserves to imply adjacent sites with zero potential play the essential role. Namely, the occupation number on adjacent sites with zero potential in the chains suggests that the emergence of the intertwined string orders are enabled by the pairing mechanism of fracton [60–64].

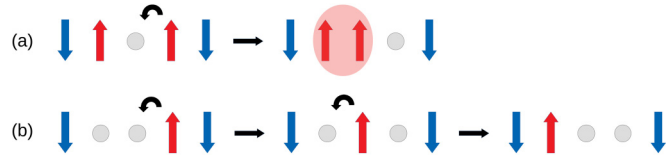

FIG. 14. Schematic of motions of a single excitation and paired excitations in a 1D antiferromagnetic chain. A pair of excitations sketched in (b) can move smoother than a single excitation in (a) [60].

Fracton is a novel topological elementary excitation in fractal structures with dimension-limited mobility. Figure 14 illustrates the motions of excitations in a 1D antiferromagnetic chain as an example of fracton mechanism. In our situation, the spin will be oriented in the X direction for the sites with $\mu = 0$, and in the Z direction for the other sites. A single spin in the X direction is not perfectly immobile but less mobile than paired spins. So, we suggest that adjacent sites with zero potential can form a fracton pair which may make it easier to host a long-range X-string order giving rise to the intertwined string orders. Hence, the degeneracy of the ground states is lifted and the TSC phase turns into the trivial phase with four nondegenerate low-lying states. Here in this work, we do not consider to calculate the dc conductivity on the lattice, so we are currently not able to determine whether the topologically trivial phase is explicitly the fracton phase. More investigations are reserved for future dynamic researches.

IV. CONCLUSION

In summary, we have studied the interacting Kitaev chains with periodic and quasiperiodic chemical potential by using the variational matrix product state (VMPS) method. In our innovative way to introduce the nonuniform chemical potential, we calculate the edge correlation function G_{1L} and find an emergent topologically trivial phase. Notably, symmetry is spontaneously broken in the topological superconducting (TSC) phase which is then split into two branches. This appealing phenomenon together with the intertwined string orders can be found in all the considered cases of spatially varying potentials. The two lowest states in each parity sector and occupation number are also calculated. The adjacent sites with zero chemical potential might be the key ingredient for the emergent phase.

ACKNOWLEDGMENTS

The authors gratefully acknowledge support from the Key Research and Development Project of Guangdong Province (Grant No. 2020B0303300001), National Natural Science Foundation of China (Grant No. 11974118), Guangdong-Hong Kong-Macao Joint Laboratory of Optoelectronic and Magnetic Functional Materials program (Grant No. 2019B121205002), and Fundamental Research Funds for the Central Universities (Grant No. 2019ZD51).

[1] C. Beenakker, Annu. Rev. Condens. Matter Phys. **4**, 113 (2013).
[2] S. R. Elliott and M. Franz, Rev. Mod. Phys. **87**, 137 (2015).
[3] M. Leijnse and K. Flensberg, Semicond. Sci. Technol. **27**, 124003 (2012).
[4] F. Wilczek, Nat. Phys. **5**, 614 (2009).
[5] D. A. Ivanov, Phys. Rev. Lett. **86**, 268 (2001).
[6] J. Alicea, Rep. Prog. Phys. **75**, 076501 (2012).
[7] C. Nayak, S. H. Simon, A. Stern, M. Freedman, and S. Das Sarma, Rev. Mod. Phys. **80**, 1083 (2008).
[8] A. Y. Kitaev, Phys. Usp. **44**, 131 (2001).
[9] S. Das Sarma, C. Nayak, and S. Tewari, Phys. Rev. B **73**, 220502(R) (2006).
[10] G. Moore and N. Read, Nucl. Phys. B **360**, 362 (1991).
[11] L. Fu and C. L. Kane, Phys. Rev. Lett. **100**, 096407 (2008).
[12] Y. Oreg, G. Refael, and F. von Oppen, Phys. Rev. Lett. **105**, 177002 (2010).
[13] R. M. Lutchyn, J. D. Sau, and S. Das Sarma, Phys. Rev. Lett. **105**, 077001 (2010).
[14] J. D. Sau, R. M. Lutchyn, S. Tewari, and S. Das Sarma, Phys. Rev. Lett. **104**, 040502 (2010).
[15] S. Tewari, J. D. Sau, and S. Das Sarma, Ann. Phys. **325**, 219 (2010).
[16] J. Alicea, Phys. Rev. B **81**, 125318 (2010).
[17] T.-P. Choy, J. M. Edge, A. R. Akhmerov, and C. W. J. Beenakker, Phys. Rev. B **84**, 195442 (2011).
[18] S. Nadj-Perge, I. K. Drozdov, B. A. Bernevig, and A. Yazdani, Phys. Rev. B **88**, 020407(R) (2013).
[19] V. Mourik, K. Zuo, S. M. Frolov, S. Plissard, E. P. Bakkers, and L. P. Kouwenhoven, Science **336**, 1003 (2012).
[20] L. P. Rokhinson, X. Liu, and J. K. Furdyna, Nat. Phys. **8**, 795 (2012).
[21] A. Das, Y. Ronen, Y. Most, Y. Oreg, M. Heiblum, and H. Shtrikman, Nat. Phys. **8**, 887 (2012).
[22] M. Deng, C. Yu, G. Huang, M. Larsson, P. Caroff, and H. Xu, Nano Lett. **12**, 6414 (2012).
[23] H. O. H. Churchill, V. Fatemi, K. Grove-Rasmussen, M. T. Deng, P. Caroff, H. Q. Xu, and C. M. Marcus, Phys. Rev. B **87**, 241401(R) (2013).
[24] E. J. Lee, X. Jiang, M. Houzet, R. Aguado, C. M. Lieber, and S. De Franceschi, Nat. Nanotechnol. **9**, 79 (2014).
[25] S. Nadj-Perge, I. K. Drozdov, J. Li, H. Chen, S. Jeon, J. Seo, A. H. MacDonald, B. A. Bernevig, and A. Yazdani, Science **346**, 602 (2014).
[26] M.-X. Wang, C. Liu, J.-P. Xu, F. Yang, L. Miao, M.-Y. Yao, C. Gao, C. Shen, X. Ma, X. Chen *et al.*, Science **336**, 52 (2012).
[27] J.-P. Xu, M.-X. Wang, Z. L. Liu, J.-F. Ge, X. Yang, C. Liu, Z. A. Xu, D. Guan, C. L. Gao, D. Qian, Y. Liu, Q. H. Wang, F. C. Zhang, Q. K. Xue, J. F. Jia *et al.*, Phys. Rev. Lett. **114**, 017001 (2015).
[28] H.-H. Sun, K.-W. Zhang, L.-H. Hu, C. Li, G.-Y. Wang, H.-Y. Ma, Z.-A. Xu, C.-L. Gao, D.-D. Guan, Y.-Y. Li, C. Liu, D. Qian, Y. Zhou, L. Fu, S. C. Li, F. C. Zhang, and J. F. Jia, Phys. Rev. Lett. **116**, 257003 (2016).
[29] H. Katsura, D. Schuricht, and M. Takahashi, Phys. Rev. B **92**, 115137 (2015).
[30] E. Sela, A. Altland, and A. Rosch, Phys. Rev. B **84**, 085114 (2011).
[31] F. Hassler and D. Schuricht, New J. Phys. **14**, 125018 (2012).
[32] R. Thomale, S. Rachel, and P. Schmitteckert, Phys. Rev. B **88**, 161103(R) (2013).
[33] S. Gangadharaiah, B. Braunecker, P. Simon, and D. Loss, Phys. Rev. Lett. **107**, 036801 (2011).
[34] T. Ohta, S. Tanaka, I. Danshita, and K. Totsuka, Phys. Rev. B **93**, 165423 (2016).
[35] T. Ohta, S. Tanaka, I. Danshita, and K. Totsuka, J. Phys. Soc. Jpn. **84**, 063001 (2015).

[36] I. Mahyaeh and E. Ardonne, J. Phys. Commun. **2**, 045010 (2018).
[37] E. M. Stoudenmire, J. Alicea, O. A. Starykh, and M. P. A. Fisher, Phys. Rev. B **84**, 014503 (2011).
[38] R. Wakatsuki, M. Ezawa, Y. Tanaka, and N. Nagaosa, Phys. Rev. B **90**, 014505 (2014).
[39] F. Crépin, G. Zaránd, and P. Simon, Phys. Rev. B **90**, 121407(R) (2014).
[40] P. W. Brouwer, M. Duckheim, A. Romito, and F. von Oppen, Phys. Rev. Lett. **107**, 196804 (2011).
[41] A. M. Lobos, R. M. Lutchyn, and S. Das Sarma, Phys. Rev. Lett. **109**, 146403 (2012).
[42] W. DeGottardi, D. Sen, and S. Vishveshwara, Phys. Rev. Lett. **110**, 146404 (2013).
[43] A. Altland, D. Bagrets, L. Fritz, A. Kamenev, and H. Schmiedt, Phys. Rev. Lett. **112**, 206602 (2014).
[44] W. DeGottardi, M. Thakurathi, S. Vishveshwara, and D. Sen, Phys. Rev. B **88**, 165111 (2013).
[45] M. Tezuka and N. Kawakami, Phys. Rev. B **85**, 140508(R) (2012).
[46] A. Manolescu, D. Marinescu, and T. D. Stanescu, J. Phys.: Condens. Matter **26**, 172203 (2014).
[47] I. Mahyaeh and E. Ardonne, Phys. Rev. B **101**, 085125 (2020).
[48] O. Motrunich, K. Damle, and D. A. Huse, Phys. Rev. B **63**, 224204 (2001).
[49] X. Cai, L.-J. Lang, S. Chen, and Y. Wang, Phys. Rev. Lett. **110**, 176403 (2013).
[50] I. I. Satija and G. G. Naumis, Phys. Rev. B **88**, 054204 (2013).
[51] M. Y. Azbel, Zh. Eksp. Teor. Fiz. **46**, 929 (1964) [JETP **19**, 634 (1964)].
[52] L.-J. Lang and S. Chen, Phys. Rev. B **86**, 205135 (2012).
[53] G. G. Naumis and F. López-Rodríguez, Phys. B: Condens. Matter **403**, 1755 (2008).
[54] Y. E. Kraus and O. Zilberberg, Phys. Rev. Lett. **109**, 116404 (2012).
[55] M. Kohmoto, L. P. Kadanoff, and C. Tang, Phys. Rev. Lett. **50**, 1870 (1983).
[56] M. Kohmoto, B. Sutherland, and C. Tang, Phys. Rev. B **35**, 1020 (1987).
[57] R. Ghadimi, T. Sugimoto, and T. Tohyama, J. Phys. Soc. Jpn. **86**, 114707 (2017).
[58] N. M. Gergs, L. Fritz, and D. Schuricht, Phys. Rev. B **93**, 075129 (2016).
[59] J.-J. Miao, H.-K. Jin, F.-C. Zhang, and Y. Zhou, Sci. Rep. **8**, 488 (2018).
[60] J. Sous and M. Pretko, Phys. Rev. B **102**, 214437 (2020).
[61] R. M. Nandkishore and M. Hermele, Annu. Rev. Condens. Matter Phys. **10**, 295 (2019).
[62] Y. You and F. von Oppen, Phys. Rev. Research **1**, 013011 (2019).
[63] S. Vijay, J. Haah, and L. Fu, Phys. Rev. B **92**, 235136 (2015).
[64] H. B. Xavier and R. G. Pereira, Phys. Rev. B **103**, 085101 (2021).
[65] P. E. de Brito, C. A. A. da Silva, and H. N. Nazareno, Phys. Rev. B **51**, 6096 (1995).
[66] Y. E. Kraus and O. Zilberberg, Nat. Phys. **12**, 624 (2016).
[67] U. Schollwöck, Ann. Phys. **326**, 96 (2011).
[68] M. Fishman, S. R. White, and E. M. Stoudenmire, arXiv:2007.14822.
[69] H. Saberi, A. Weichselbaum, and J. von Delft, Phys. Rev. B **78**, 035124 (2008).
[70] T. Ohta and K. Totsuka, J. Phys. Soc. Jpn. **85**, 074003 (2016).
[71] M. McGinley, J. Knolle, and A. Nunnenkamp, Phys. Rev. B **96**, 241113(R) (2017).
[72] A. Rahmani, X. Zhu, M. Franz, and I. Affleck, Phys. Rev. B **92**, 235123 (2015).
[73] S. V. Aksenov, A. O. Zlotnikov, and M. S. Shustin, Phys. Rev. B **101**, 125431 (2020).
[74] C. Monthus, J. Phys. A: Math. Theor. **51**, 465301 (2018).
[75] J.-J. Miao, H.-K. Jin, F.-C. Zhang, and Y. Zhou, Phys. Rev. Lett. **118**, 267701 (2017).
[76] G. Kells, Phys. Rev. B **92**, 081401(R) (2015).
[77] G. Goldstein and C. Chamon, Phys. Rev. B **86**, 115122 (2012).
[78] W. DeGottardi, D. Sen, and S. Vishveshwara, New J. Phys. **13**, 065028 (2011).
[79] K. Wada, T. Sugimoto, and T. Tohyama, Phys. Rev. B **104**, 075119 (2021).
[80] Z.-Y. Zheng, H.-C. Kou, and P. Li, Phys. Rev. B **100**, 235127 (2019).
[81] K. Kawabata, R. Kobayashi, N. Wu, and H. Katsura, Phys. Rev. B **95**, 195140 (2017).
[82] J. Wouters, H. Katsura, and D. Schuricht, Phys. Rev. B **98**, 155119 (2018).
[83] R. Diehl, J. Ledieu, N. Ferralis, A. Szmodis, and R. Mcgrath, J. Phys.: Condens. Matter **15**, R63 (2003).